NANO LETTERS

Letter

pubs.acs.org/NanoLett

Nanometer Thick Elastic Graphene Engine

Jong Hak Lee,*[,†,‡] Jun You Tan,[‡] Chee-Tat Toh,[†,‡] Steven P. Koenig,[†,‡] V. E. Fedorov,[∥] Antonio H. Castro Neto,[†,‡] and Barbaros Özyilmaz*[,†,‡,§]

[†]Department of Physics, National University of Singapore, 117542 Singapore

[‡]Graphene Research Center, National University of Singapore, 117542 Singapore

[§]NanoCore, National University of Singapore, 117576 Singapore

[∥]Nikolaev Institute of Inorganic Chemistry, Siberian Branch of Russian Academy of Sciences 3, Acad. Lavrentiev prospect, Novosibirsk 630090, Russia

S *Supporting Information*

ABSTRACT: Significant progress has been made in the construction and theoretical understanding of molecular motors because of their potential use. Here, we have demonstrated fabrication of a simple but powerful 1 nm thick graphene engine. The engine comprises a high elastic membrane-piston made of graphene and weakly chemisorbed ClF_3 molecules as the high power volume changeable actuator, while a 532 nm LASER acts as the ignition plug. Rapid volume expansion of the ClF_3 molecules leads to graphene blisters. The size of the blister is controllable by changing the ignition parameters. The estimated internal pressure per expansion cycle of the engine is about ~10^6 Pa. The graphene engine presented here shows exceptional reliability, showing no degradation after 10 000 cycles.

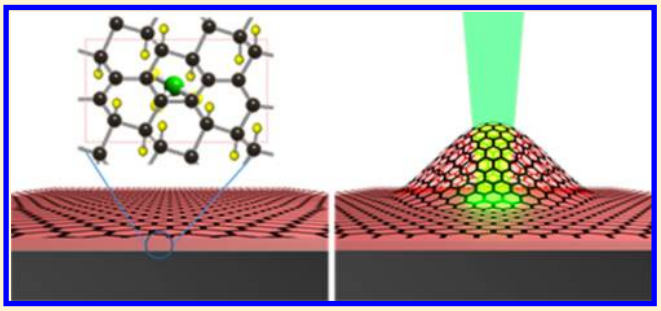

KEYWORDS: *Graphene, nanomechanics, graphite intercalation compound, graphene blister*

Micro- and nanosized motors and rotors have attracted a great deal of interest because of their potential use in micro/nano machine applications.[1−8] Significant progress has been made in the construction and theoretical understanding of molecular motors because of their potential use.[1−8] The design of an artificial molecular engine often takes inspiration from their macroscopic counterparts.[9−11] However, existing molecular motors are typically powered by quantum[3−5] or catalytic chemical processes.[6,7] To date, there is no report for conventional internal heat engine on the nanometer scale despite the widespread use of 2- and 4-stroke engines since the 19th century. In this work, we suggest a new type of ultrathin graphene engine, which mimics the heat engine system. Such an engine is composed of graphene and the weakly chemisorbed ClF_3 molecules as the recyclable high power volume changeable actuator. A LASER (light amplification by stimulated emission of radiation) beam is used as a local "ignition plug". Sublimation of the ClF_3 molecules upon illuminating with the LASER beam leads to a rapid volume expansion at the interface between graphene and the substrate thus generating high pressure and forming a dome-like blister. By changing the sublimation parameter, the size of the blister can be controlled. The obtained gasification pressure of the graphene engine during one cycle is approximately 22.9 MPa. The graphene engine presented here shows exceptional reliability, showing no degradation after 10 000 cycles.

Figure 1 illustrates the basic structure and operating principle of our graphene engine, which was constructed from exfoliated ClF_3 intercalated graphite. The intercalated graphite has ionic C−F bonds between ClF_3 molecules and the graphene layer, which can be easily dissociated.[12] The ClF_3 molecules lose their ionic bond with graphene upon exposing to a 532 nm LASER beam. This leads to a rapid increase in pressure and delaminates graphene from the substrate. The increase in volume in turn leads to formation of a blister (Figure 1a). This has been directly measured by simultaneously monitoring the Raman spectrum (Figure 1b). After the LASER is turned off, graphene goes back to its original flat state because the high reactivity of ClF_3 molecules chemisorb back onto the graphene. The rapid increase in pressure followed by the volume expansion and contraction under the graphene sheet are equivalent to the explosion and motion of the piston of an internal combustion engine. Key to the performance of a graphene-based engine is that the high pressure between the substrate and graphene can be sustained due to its high Young's modulus,[13] gas impermeability,[14] and high adhesion energy.[15]

The liquid ClF_3 treated graphite intercalation compound has ionic C−F bonds between ClF_3 molecules and the graphene

Received: February 13, 2014
Revised: April 22, 2014
Published: April 28, 2014

   dx.doi.org/10.1021/nl500568d | *Nano Lett.* 2014, 14, 2677−2680

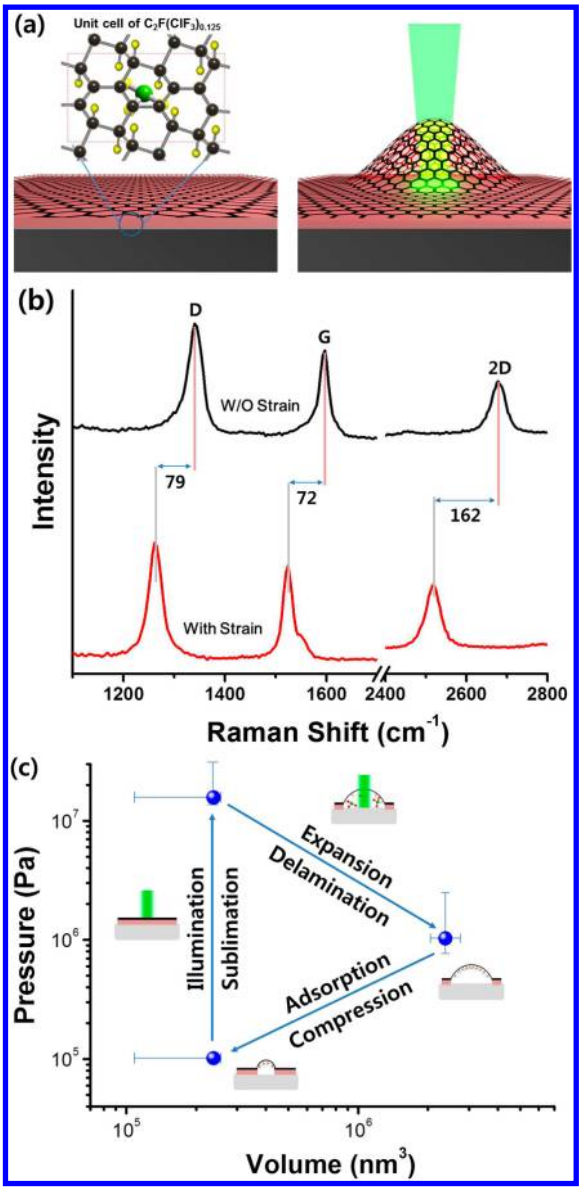

Figure 1. Schematics of graphene engine and its cycling property. (a) The rapid volume expansion of ClF_3 molecules by photon energy makes high internal pressure and leads graphene membrane to bulge upward like a blister. (b) There are large red shifts of graphene engine on D, G, and 2D peaks compared to those of the nonstrained graphene engine. The obtained strain of graphene is $\varepsilon = 1.16\%$. (c) After recondensation of ClF_3 molecules on graphene because of its high fluorinating reactivity, the p_{in} simultaneously decreased then the highly elastic graphene engine goes back to its original flat state.

layer resulting in a charge transfer of 1/6 of a hole per fluorine atom.[12] The ionic C−F bond can be easily dissociated because the bond dissociation energy (BDE) is approximately 54 kJ/mol.[12] This is much smaller than that reported for covalent C−F bonds (~460 kJ/mol).[12] Hence, the temporarily stabilized ClF_3 molecules lose their ionic bond with graphene upon exposing to a LASER beam leading to gasification of the ClF_3 molecules and a rapid pressure increase. Using the combination of ideal gas law and Hencky's solutions, a lower bound for the deduced initial internal pressure during one rapid volume expansion is 22.9 MPa (see Supporting Information). Such high internal pressure is sufficient to locally delaminate graphene from the substrate. In order to investigate the internal pressure more quantitatively after the expansion process, we used Hencky's solution for volume of the blister ($V_b = C_1(\nu)\pi\delta(\alpha/2)^2$), where ν is Poisson's ratio, the $C_1(\nu)$ is the coefficient that depends only on ν, δ is the maximum deflection, and α is the diameter of the blister. For graphene, we used $\nu = 0.16$ so $C_1(\nu = 0.16) = 0.524$[15] and obtained V_b and internal pressure (p_{in}) of the graphene blister to be approximately 3×10^6 nm^3 and 1.15 MPa, respectively (see Supporting Information). After the LASER is turned off, the ClF_3 molecules chemisorb to the graphene because of its high reactivity.[16] The functionalization and intercalation of graphite using ClF_3 gas have been experimentally demonstrated by Nazarov and Makotchenko.[17,18] In addition, the ClF_3 molecule itself is stable until 300 °C (at 300 °C, 3% of ClF_3 can be decomposed with formation of ClF and F_2; even that reaction is reversible depending on the temperature).[18] This implies that such a functionalized graphene engine potentially could be reliable for a high number of cycles.

The strain of graphene can be easily estimated by Raman spectroscopy.[19−22] Using the values reported of the Gruneisen parameter (γ) by Zabel et al.,[23] we have estimated the strain on graphene in our "graphene engine" during the process of rapid volume expansion to be 1.16% (see Supporting Information). The pressure difference Δp across the membrane (at the interface and outside) of the blister model can be estimated by using the following relationship: $\Delta p = C_2(\nu)Et[\delta^3/(\alpha/2)^4]$, where ν is Poisson's ratio, $C_2(\nu)$ is a coefficient that depends only on ν, E is the Young's modulus, and t is the thickness of the membrane.[24,25] In order to map the blister profile (deflection δ and blister diameter α) of the graphene, we have performed Raman line scan and blister bursting test. Using the line scan mode of Raman spectroscopy, we scanned from inside the graphene flake to the edge, on the graphene engine. It traced spots along the designated line. For each traced spot, we match the Raman shift result and the AFM result to see the trend in both. Within the diameter of the blister, if and when it faces a ripple or the edge of graphene flake, we assume that the blister has less strain due to leakage of ClF_3 molecules or pinning at the edge. Accordingly, the Raman spectrum is less red-shifted. The trace of LASER spot is easily distinguished in AFM phase image. As shown in Figure 2a, the spots 5 (ripple) and 8 (edge) have less red-shifted Raman spectra compared to that of the normal spot. Using red-shifted Raman result differences, we roughly deduced the size of the blister with various LASER power. The diameter of the blister with 0.32 mW LASER power is about 550 nm (see Supporting Information for various LASER power). However, the bursting of the blister is achieved by repeatedly cycling the LASER light exposure under severe working conditions (more than 8.5 mW of LASER power). It has been experimentally demonstrated that the LASER irradiation can induce defects on graphene.[26] We assume that when the rapid gasification of ClF_3 molecules generates high-enough pressure from underneath graphene, the LASER induced point defect nucleates at the center and then the crack will be propagated until the edge of the blister. Figure 2b shows the Raman spectrum difference before and after the bursting of the blister. The rapid volume expansion-induced strain on graphene has been monitored until the 363th cycle. However, during the 364th cycle, Raman signatures suddenly shifted back to their original positions. The internal pressure seems to have torn the graphene membrane allowing the gasified ClF_3 molecules to escape from the graphene blister releasing in the process the strain on graphene. Following this,

dx.doi.org/10.1021/nl500568d | Nano Lett. 2014, 14, 2677−2680

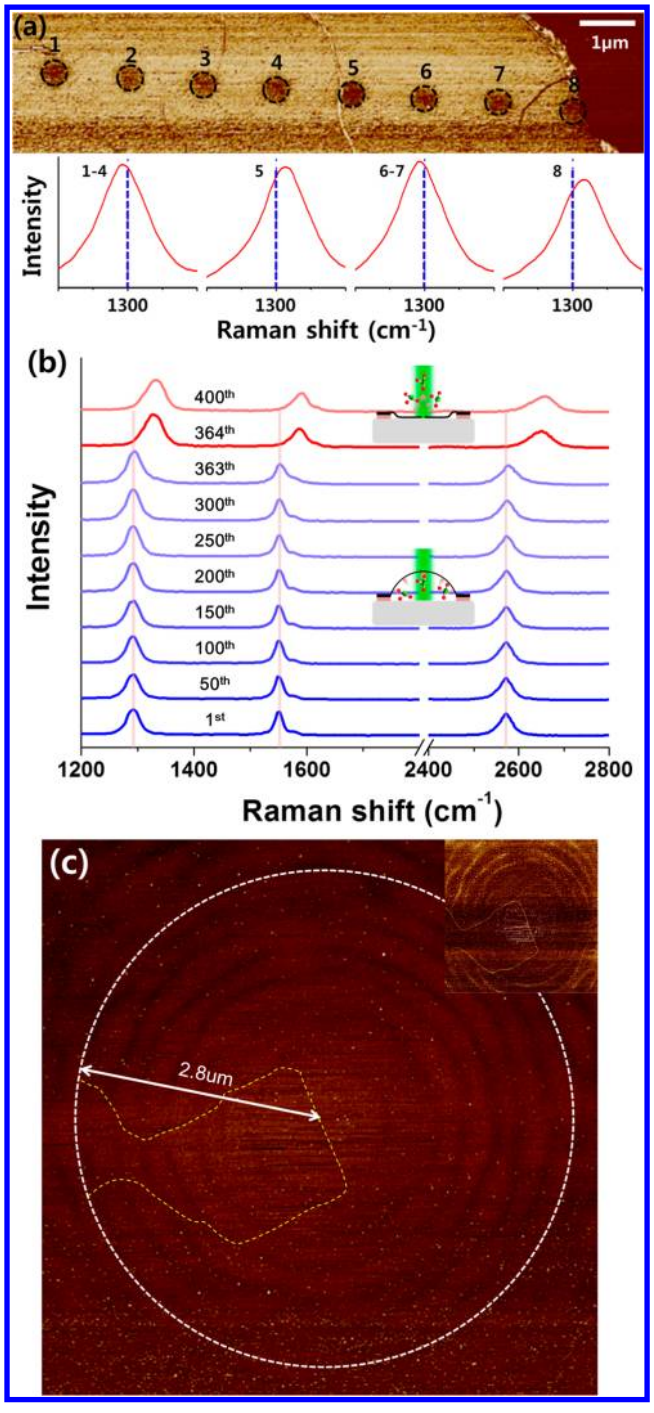

Figure 2. Raman line scan and blister bursting test (BBT) for blister profile investigation. (a) Because of the leak of ClF_3 molecules and pinning effect at the edge, the blister has less strain when the blister faces the ripple or edge of the graphene engine. Using red-shifted Raman result differences, we deduced the diameter of the blister to be 550 nm. (b) For the BBT, internal rapid volume expansion was repeated. At the 364th cycle, the graphene engine was broken and the red-shifted peaks came back to their normal position (without strain). Inset schematics show the relevant situation of the graphene engine to Raman results. (c) The broken graphene engine has the crack with 2.8 μm as radius. Inset clearly shows a crack on the graphene engine.

we performed atomic force microscopy (AFM) at the same location to check the extension of the crack. As shown in Figure 2c, the AFM phase image clearly indicates a crack on graphene. Using the values $\nu = 0.16$, $C_2(\nu) = 3.09$, $Et = 347$ N/m (in this calculation, we used the same value of graphene for Et; even after functionalization, the Et value is approximately similar to that of graphene because as Young's modulus decreased, the thickness also increased), $\alpha/2 = 2.8$ μm, and $\delta = 325$ nm we obtained the relationship of strain and diameter.[15] The estimated Δp is ~0.6 MPa, and the internal pressure of graphene blister is approximately $p_{in} = 0.7$ MPa. The obtained internal pressure values of graphene blister from two different ways such as combination of ideal gas law, line scan Raman spectra, and blister burst test are quite similar as 0.7−1.15 MPa. Therefore, we deduced that the high internal pressure generated by LASER illumination induces varied deflection and delamination on the graphene depending on the LASER power (Figure 3a). Finally, the graphene blister has stable shape

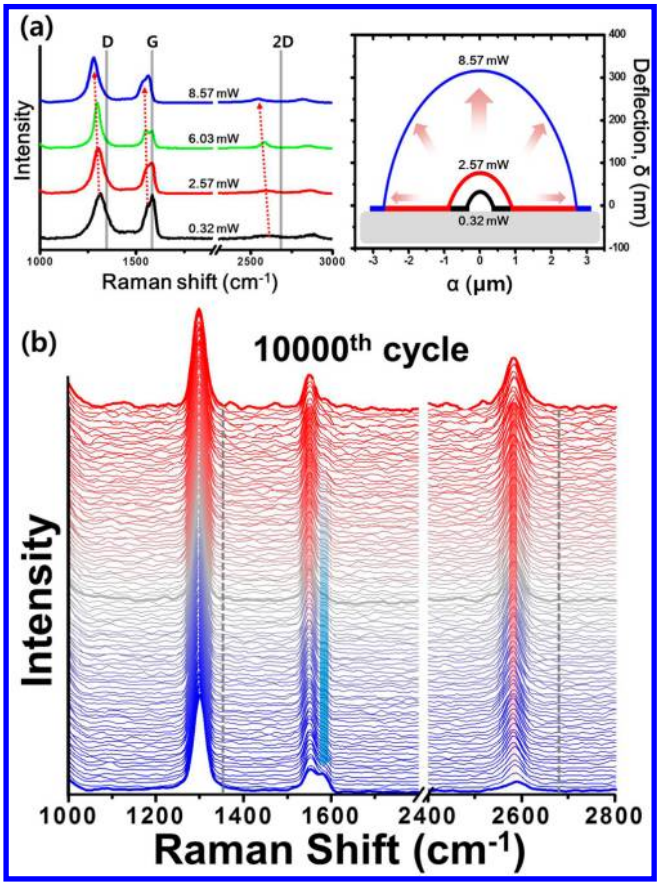

Figure 3. Raman characterization results for the graphene blister size control and the sustainability test. (a) Raman results of graphene engine according to the laser power and its relevant scheme based on the line scan Raman spectroscopy measurement and BBT results. (b) After elimination of point defect nucleation by reducing the LASER power, we obtained a sustainable graphene engine even after the 10 000th volume expansion cycle. As volume expansion cycles go by (from botton to top), fluorine-functionalized graphene has been reduced. G and 2D peaks evolved, and D′ peak was reduced (all graphs are normalized by D peak intensity).

when internal pressure and adhesion energy of graphene are in equilibrium state. An adhesion energy of 0.127 J/m^2 is calculated, which is in-line with previous results (see Supporting Information). It should be noted that the adhesion energy is slightly lower than that of graphene to SiO_2, but this is expected due to the presence of the intercalated ClF_3 molecules. To investigate the durability of the engine, we

dx.doi.org/10.1021/nl500568d | Nano Lett. 2014, 14, 2677−2680

have eliminated the point defect nucleation by simply reducing the LASER power and repeated the volume expansion cycle at least up to 10 000 times. As shown in Figure 3b, we did not observe the Raman signatures shifting back to their original positions even after the 10 000th volume expansion cycle. It is possible to make the sustainable working condition of the graphene engine with high power by choosing appropriate LASER power and LASER spot size, which have a significant advantage, thus optimizing the engine's efficiency and performance according to the need. Further work would be necessary to understand the rapid volume expansion state with high LASER power and to improve the engine by exploring various other possible volume changeable actuators, how to connect the engine to the target load, on/off speed test, illumination parameters such as beam size, photon energy, the design, etc.

In conclusion, we have demonstrated a new type of graphene engine made from nanometer thick fluorinated graphene. The main components of our engine are (fluorinated) graphene for high-elastic piston, chemisorbed ClF_3 molecules for recyclable high-power volume changeable actuator, and a LASER source of wavelength 532 nm as the "ignition plug". By changing the sublimation parameter (i.e., LASER power), we optimized the sustainable working condition with high power generation. We have investigated our graphene-based elastic engine by performing a blister bursting test. The estimated gasification pressure is at least 22.9 MPa, and at such a high pressure, the engine could reversibly sustain the rapid volume expansion more than 10 000 cycles by fine-tuning the illumination energy. Graphene's high Young's modulus, ultrastrong adhesion, and gas impermeability make the engine highly energy efficient and durable. We believe that this work opens up a new avenue to explore novel applications of graphene and alternative micro/nano engine for the next generation devices.

■ ASSOCIATED CONTENT

Supporting Information

Experimental, additional AFM and photo images, and additional measurements. This material is available free of charge via the Internet at http://pubs.acs.org.

■ AUTHOR INFORMATION

Corresponding Authors

*(J.H.L.) E-mail: ljhacy@gmail.com.
*(B.O.) E-mail: phyob@nus.edu.sg.

Notes

The authors declare no competing financial interest.

■ ACKNOWLEDGMENTS

We thank Dr. V. Makotchenko for help in synthetic work and Dr. Vitor Pereira and Dr. Shaffique Adam for discussions. This research is supported by the National Research Foundation, Prime Minister's Office, Singapore, under its Competitive Research Programme (CRP Award No. NRF-CRP9-2011-3 and NRF-CRP6-2010-5), Research Fellowship (RF Award No. 224 NRF-RF2008-7), NUS Young Investigator Award, and SMF-NUS Research Horizons Award 2009-Phase II.

■ REFERENCES

(1) Bath, J.; Turberfield, A. J. *Nat. Nanotechnol.* **2007**, *2*, 275−284.
(2) Goel, A.; Vogel, V. *Nat. Nanotechnol.* **2008**, *8*, 465−475.
(3) van Delden, R. A.; ter Wiel, M. K. J.; Pollard, M. M.; Vicario, J.; Koumura, N.; Feringa, B. L. *Nature* **2005**, *437*, 1337−1340.
(4) Liu, M.; Zentgraf, T.; Liu, Y. M.; Bartel, G.; Zhang, X. *Nat. Nanotechnol.* **2010**, *8*, 570−573.
(5) Ruangsupapichat, N.; Pollard, M. M.; Harutyunyan, S. R.; Feringa, B. L. *Nat. Chem.* **2011**, *3*, 53−60.
(6) Chen, L.; Nakamura, M.; Schindler, T. D.; Parker, D.; Bryant, Z. *Nat. Nanotechnol.* **2012**, *7*, 252−256.
(7) Lee, L. K.; Ginsburg, M. A.; Crovace, C.; Donohoe, M.; Stock, D. *Nature* **2010**, *466*, 996−1000.
(8) Tierney, H. L.; Murphy, C. J.; Jewell, A. D.; Baber, A. E.; Iski, E. V.; Khodaverdian, H. Y.; McGuire, A. F.; Klebanov, N.; Sykes, E. C. H. *Nat. Nanotechnol.* **2011**, *6*, 625−629.
(9) Kudernac, T.; Ruangsupapichat, N.; Parschau, M.; Maciá, B.; Katsonis, N.; Harutyunyan, S. R.; Ernst, K.-H.; Feringa, B. L. *Nature* **2011**, *479*, 208−211.
(10) Manzano, C.; Soe, W. H.; Wong, H. S.; Ample, F.; Gourdon, A.; Chandrasekhar, N.; Joachim, C. *Nat. Mater.* **2009**, *8*, 576−579.
(11) Wickham, S. F. J.; Endo, M.; Katsuda, Y.; Hidaka, K.; Bath, J.; Sugiyama, H.; Turberfield, A. J. *Nat. Nanotechnol.* **2011**, *6*, 166−169.
(12) di Vittorio, S. L.; Dresselhaus, M. S.; Dresselhaus, G. *J. Mater. Res.* **1993**, *8*, 1578−1585.
(13) Lee, C. G.; Wei, X.; Kysar, J. W.; Hone, J. *Science* **2008**, *321*, 385−388.
(14) Bunch, J. S.; Verbridge, S. S.; Alden, J. S.; Zande, A. M. v. d.; Parpia, J. M.; Craighead, H. G.; McEuen, P. L. *Nano Lett.* **2008**, *8*, 2458−2462.
(15) Steven, P. K.; Narasimha, G. B.; Martin, L. D.; Bunch, J. S. *Nat. Nanotechnol.* **2011**, *6*, 543−546.
(16) Simons, J. H. *Fluorine Chemistry*; Academic Press: New York, 1965; p 39.
(17) Makotchenko, V. G.; Nazarov, A. S.; Yakovlev, I. I. *Dokl. Chem.* **2001**, *380*, 252−254.
(18) Nazarov, A. S.; Makotchenko, V. G. *Inorg. Mater.* **2001**, *38*, 278−282.
(19) Mohiuddin, T. M. G.; Lombardo, A.; Nair, R. R.; Bonetti, A.; Savini, G.; Jalil, R.; Bonini, N.; Basko, D. M.; Galiotis, C.; Marzari, N.; Novoselov, K. S.; Geim, A. K.; Ferrari, A. C. *Phys. Rev. B* **2009**, *79*, 205433−205440.
(20) Mohr, M.; Maultzsch, J.; Thomsen, C. *Phys. Rev. B* **2010**, *82*, 201409(R).
(21) Ding, F.; Ji, H.; Chen, Y.; Herklotz, A.; Dorr, K.; Mei, Y.; Rastelli, A.; Schmidt, O. G. *Nano Lett.* **2010**, *10*, 3453−3458.
(22) Metzger, C.; Remi, S.; Liu, M.; Kusminskiy, S. V.; Castro Neto, A. H.; Swan, A. K.; Goldberg, B. B. *Nano Lett.* **2010**, *10*, 6−10.
(23) Zabel, J.; Nair, R. R.; Ott, A.; Georgiou, T.; Geim, A. K.; Novoselov, K. S.; Casiraghi, C. *Nano Lett.* **2012**, *12*, 617−621.
(24) Hencky, H. *Math. Phys.* **1915**, *63*, 311−317.
(25) Williams, J. *Int. J. Fract.* **1997**, *87*, 265−288.
(26) Krauss, B.; Lohmann, T.; Chae, D. H.; Haluska, M.; von Klitzing, K.; Smet, J. H. *Phys. Rev. B* **2009**, *79*, 165428(16).